
Scalable Cross Validation Losses for Gaussian Process Models

Martin Jankowiak

Broad Institute

Cambridge, Massachusetts, USA

mjankowi@broadinstitute.org

Geoff Pleiss

Columbia University

New York City, New York, USA

gmp2162@columbia.edu

Abstract

We introduce a simple and scalable method for training Gaussian process (GP) models that exploits cross-validation and nearest neighbor truncation. To accommodate binary and multi-class classification we leverage Pólya-Gamma auxiliary variables and variational inference. In an extensive empirical comparison with a number of alternative methods for scalable GP regression and classification, we find that our method offers fast training and excellent predictive performance. We argue that the good predictive performance can be traced to the non-parametric nature of the resulting predictive distributions as well as to the cross-validation loss, which provides robustness against model mis-specification.

1 Introduction

As machine learning becomes more widely used, it is increasingly being deployed in applications where autonomous decisions are guided by predictive models. For example, supply forecasts can determine the prices charged by retailers, expected demand for transportation can be used to optimize bus schedules, and data-driven algorithms can guide load balancing in critical electrical subsystems. For these and many other applications of machine learning, it is essential that models are well-calibrated, thus enabling downstream decisions to factor in uncertainty and risk.

Gaussian processes are a general-purpose modeling component that offer excellent uncertainty quantification in a variety of predictive tasks, including regression, classification, and beyond [Rasmussen, 2003]. Despite their many attractive features, wider use of Gaussian process (GP) models is hindered by computational requirements that can be prohibitive. For example, classic methods for training GP regressors using the marginal log likelihood (MLL), also known as Type II Maximum Likelihood, scale cubically with the number of data points. This bottleneck has motivated extensive research into approximate GP inference schemes with more favorable computational properties [Liu et al., 2020].

A particularly popular and fruitful approach has centered on inducing point methods and variational inference [Snelson and Ghahramani, 2006, Titsias, 2009, Hensman et al., 2013]. These methods rely on the ELBO, which is a lower bound to the MLL, for training and trade cubic complexity in the size of the dataset N for cubic complexity in the number of inducing points M . Since M is a hyperparameter controlled by the user, inducing point methods can lead to substantial speed-ups. One disadvantage of inducing point methods—as we will see explicitly in our empirical evaluation—is that some datasets may require prohibitively large values of M to ensure good model fit.

Instead of targeting the MLL directly or via a lower bound, we investigate the suitability of training objectives based on *cross-validation* (CV). In this work we argue that CV is attractive in the context of GP models for three reasons in particular: i) it can provide robustness against model mis-specification; ii) it opens the door to simple approximation schemes based on nearest neighbor truncation; and iii) nearest neighbor truncation enables non-parametric predictive distributions that avoid some of the disadvantages of inducing point methods. To put it differently, although nearest neighbors are

a natural starting point for scalable GP methods, their combination with MLL-based objectives is typically made awkward by the need to specify an ordering of the data [Vecchia, 1988, Datta et al., 2016]. In contrast, CV-based objectives are free of any such requirement, resulting in an attractive synergy between cross-validation and nearest neighbor approximations. To exploit this synergy we make the following contributions:

1. We introduce the k -nearest-neighbor leave-one-out (**LOO-k**) objective, which can be used to train GP models on large datasets.
2. We introduce a Pòlya-Gamma auxiliary variable construction that extends this approach to binary and multi-class classification.
3. We perform an extensive empirical comparison with a number of alternative methods for scalable GP regression and classification and demonstrate the excellent predictive performance of our approach.

Before we describe our approach in Sec. 3 we first review some basic background on Gaussian processes, which also gives us the opportunity to establish some of the notation we will use throughout.

2 Background on Gaussian processes

A GP on the input space $\mathcal{D} \subset \mathbb{R}^D$ is specified¹ by a covariance function or kernel $K : \mathcal{D} \times \mathcal{D} \rightarrow \mathbb{R}$ [Rasmussen, 2003]. A common choice is the RBF or squared exponential kernel, which is given by

$$K(\mathbf{x}, \mathbf{z}) = \sigma_K^2 \exp\left\{-\frac{1}{2}\sum_i(x_i - z_i)^2/\rho_i^2\right\} \quad (1)$$

where $\{\rho_i\}$ are length scales and σ_K is the kernel scale. For scalar regression $f : \mathcal{D} \rightarrow \mathbb{R}$ the joint density of a GP takes the form

$$p(\mathbf{y}, \mathbf{f} | \mathbf{X}) = \mathcal{N}(\mathbf{y} | \mathbf{f}, \sigma_{\text{obs}}^2 \mathbb{1}_N) \mathcal{N}(\mathbf{f} | \mathbf{0}, \mathbf{K}_{N,N}) \quad (2)$$

where \mathbf{y} are the real-valued targets, \mathbf{f} are the latent function values, $\mathbf{X} = \{\mathbf{x}_i\}_{i=1}^N$ are the N inputs with $\mathbf{x}_i \in \mathcal{D}$, σ_{obs}^2 is the variance of the Normal likelihood, and $\mathbf{K}_{N,N}$ is the $N \times N$ kernel matrix. The marginal log likelihood (MLL) of the observed data can be computed in closed form:

$$\log p(\mathbf{y} | \mathbf{X}) = \log \int d\mathbf{f} p(\mathbf{y}, \mathbf{f} | \mathbf{X}) = \log \mathcal{N}(\mathbf{y}, \mathbf{K}_{N,N} + \sigma_{\text{obs}}^2 \mathbb{1}_N). \quad (3)$$

Computing $\log p(\mathbf{y} | \mathbf{X})$ has cost $\mathcal{O}(N^3)$, which has motivated the great variety of approximate methods for scalable training of GP models [Liu et al., 2020]. The posterior predictive distribution $p(y_* | \mathbf{y}, \mathbf{X}, \mathbf{x}_*)$ of the GP at a test point $\mathbf{x}_* \in \mathcal{D}$ is the Normal distribution $\mathcal{N}(\mu_f(\mathbf{x}_*), \sigma_f(\mathbf{x}_*)^2 + \sigma_{\text{obs}}^2)$ where $\mu_f(\cdot)$ and $\sigma_f(\cdot)^2$ are given by

$$\mu_f(\mathbf{x}_*) = \mathbf{K}_{*,N}^T (\mathbf{K}_{N,N} + \sigma_{\text{obs}}^2 \mathbb{1}_N)^{-1} \mathbf{y} \quad (4)$$

$$\sigma_f(\mathbf{x}_*)^2 = K_{**} - \mathbf{K}_{*,N}^T (\mathbf{K}_{N,N} + \sigma_{\text{obs}}^2 \mathbb{1}_N)^{-1} \mathbf{K}_{*,N} \quad (5)$$

Here $K_{**} = K(\mathbf{x}_*, \mathbf{x}_*)$ and $\mathbf{K}_{*,N}$ is the column vector with elements $(\mathbf{K}_{*,N})_n = K(\mathbf{x}_*, \mathbf{x}_n)$.

3 Nearest neighbor cross-validation losses

The marginal log likelihood of a GP can be written as a sum of logs of univariate posterior conditionals, where for a fixed, arbitrary ordering $\{1, \dots, N\}$ we have

$$\mathcal{L}_{\text{MLL}} \equiv \log p(\mathbf{y} | \mathbf{X}) = \sum_{n=1}^N \log p(y_n | \mathbf{y}_{<n}, \mathbf{x}_{\leq n}) \quad (6)$$

and where $\mathbf{y}_{<n} \equiv \{y_1, \dots, y_{n-1}\}$ and $\mathbf{x}_{\leq n} \equiv \{\mathbf{x}_1, \dots, \mathbf{x}_n\}$.² Summing over all $N!$ permutations $\tau \in S^N$ we obtain

$$\mathcal{L}_{\text{MLL}} = \frac{1}{N!} \sum_{\tau \in S^N} \sum_{n=1}^N \log p(y_n^\tau | \mathbf{y}_{<n}^\tau, \mathbf{x}_{\leq n}^\tau) \equiv \sum_{n=0}^{N-1} \mathcal{L}_{\text{CV}}^n \quad (7)$$

¹Unless otherwise noted we assume that the prior mean is uniformly zero.

²We define $\mathbf{y}_{<1} \equiv \emptyset$. Note that here and elsewhere we suppress dependence on the kernel hyperparameters.

where τ superscripts denote application of the permutation τ .³ Additionally on the RHS of Eqn. 7 we have grouped the $N \times N!$ terms in the sum w.r.t. the number of data points that each term conditions on, i.e. each term in $\mathcal{L}_{\text{CV}}^n$ conditions on exactly n data points and is implicitly defined by Eqn. 7. For example we have

$$\mathcal{L}_{\text{CV}}^{N-1} = \frac{1}{N} \sum_{n=1}^N \log p(y_n | \mathbf{y}_{-n}, \mathbf{X}) \quad \text{and} \quad \mathcal{L}_{\text{CV}}^0 = \frac{1}{N} \sum_{n=1}^N \log p(y_n | \mathbf{x}_n) \quad (8)$$

where $\mathbf{y}_{-n} \equiv \{y_1, \dots, y_{n-1}, y_{n+1}, \dots, y_N\}$. This decomposition makes a number of properties of the marginal log likelihood apparent. First, the MLL is directly linked to the average posterior predictive performance conditioned on *all* possible training data sets, including the empty set [Fong and Holmes, 2020]. Second, the inclusion of conditioning sets that are only a small fraction of the full dataset—in the extreme case empty conditioning sets as in $\mathcal{L}_{\text{CV}}^0$ —means that \mathcal{L}_{MLL} can exhibit substantial dependence on the prior. Indeed the term $\mathcal{L}_{\text{CV}}^0$ scores the model exclusively with respect to the *prior* predictive. Conversely, $\mathcal{L}_{\text{CV}}^{N-1}$ exhibits the least dependence on the prior.

In the following we will use $\mathcal{L}_{\text{CV}}^{N-1}$ as the basis for our training objective. This choice is motivated by two observations. First, as we have just argued, we expect $\mathcal{L}_{\text{CV}}^{N-1}$ to provide robustness against prior mis-specification due to its reduced dependence on the prior. Indeed it is well known that conventional Bayesian inference can be suboptimal when the model is mis-specified: see [Masegosa, 2019] and references therein for recent discussion. Second, while $\mathcal{L}_{\text{CV}}^{N-1}$ depends on the entire dataset, *individual* predictive distributions $p(y_n | \mathbf{y}_{-n}, \mathbf{X})$ in the sum typically exhibit *non-negligible* dependence on only a small subset of the conditioning data.⁴ This latter observation opens the door to nearest neighbor truncation, which we describe next.

3.1 Nearest neighbor truncation

In the regression case (see Eqn. 4-5) computing $\mathcal{L}_{\text{CV}}^{N-1}$ in Eqn. 8 has $\mathcal{O}(N^4)$ cost if done naively, which is very expensive for $N \gtrsim 10^3$. While this can be reduced to $\mathcal{O}(N^3)$ for a stochastic estimate or if care is taken with the algebra [Petit et al., 2020, Ginsbourger and Schärer, 2021], this still precludes a training algorithm that scales to large datasets with millions of data points. To enable scalability, we apply a k -nearest-neighbor truncation to $\mathcal{L}_{\text{CV}}^{N-1}$ to obtain the k -truncated leave-one-out (**LOO-k**) objective

$$\mathcal{L}_{\text{LOO}}^k \equiv \frac{1}{N} \sum_{n=1}^N \log p(y_n | \mathbf{y}_{n,k}, \mathbf{X}_{n,k}, \mathbf{x}_n) \quad (9)$$

where we use $k = \infty$ to denote the non-truncated objective. Here the pair $(\mathbf{y}_{n,k}, \mathbf{X}_{n,k})$ denotes the k -nearest-neighbors of \mathbf{x}_n (and the corresponding targets) as determined using the Euclidean metric defined with kernel length scales ρ_i .⁵ For univariate regression computing Eqn. 9 has a $\mathcal{O}(Nk^3)$ cost. Utilizing data subsampling to obtain a stochastic estimate $\widehat{\mathcal{L}}_{\text{LOO}}^k$, this cost becomes $\mathcal{O}(Bk^3)$ for mini-batch size B . Notably, the bottleneck in computing $\widehat{\mathcal{L}}_{\text{LOO}}^k$ involves a batch Cholesky decomposition of a $B \times k \times k$ tensor, which can be done extremely efficiently on a GPU for $k \lesssim 500$ even for $B \sim 100$. The nearest neighbor search takes $\mathcal{O}(N \log N)$ time using standard algorithms like k-d trees [Bentley, 1975], though for $N \lesssim 10^7$ it is often faster to use $\mathcal{O}(N^2)$ brute force algorithms that make use of GPU parallelism.⁶ In practice we recompute the nearest neighbor index somewhat infrequently, e.g. after every 50th gradient update. See Algorithm 1 in the supplemental materials for a summary of the training procedure.

³For example $y_n^\tau \equiv y_{\tau(n)}$ and $\mathbf{y}_{<n}^\tau \equiv \{y_{\tau(1)}, \dots, y_{\tau(n-1)}\}$

⁴At least for approximately compactly-supported kernels like RBF or Matérn. Our method is not immediately applicable to, e.g., periodic kernels as are commonly used in time-series applications.

⁵That is we compute nearest neighbors w.r.t. the distance function $d(\mathbf{x}, \mathbf{z}) = \sqrt{\sum_i (x_i - z_i)^2 / \rho_i^2}$. Note that by definition $\mathbf{X}_{n,k}$ does *not* contain \mathbf{x}_n .

⁶Modern nearest neighbor libraries, e.g. FAISS [Johnson et al., 2019], perform nearest neighbor searches in a map-reduce fashion. This yields a $\mathcal{O}(N)$ memory requirement, which is feasible on a single GPU for $N \lesssim 10^7$. For larger datasets it is possible to achieve speed-ups with quantization, trading off speed for accuracy.

To make a prediction for a test point \mathbf{x}_* we simply compute the k -truncated posterior predictive distribution $p(y_n|\mathbf{y}_{*,k}, \mathbf{X}_{*,k}, \mathbf{x}_*)$. Here the nearest neighbors $(\mathbf{y}_{*,k}, \mathbf{X}_{*,k})$ are formed using a pre-computed nearest neighbor index that only needs to be computed once. The nearest neighbor query takes $\mathcal{O}(N)$ time using a brute force index and $\mathcal{O}(\log N)$ time for a k-d tree. The cost of forming the predictive distribution is then $\mathcal{O}(k^3)$. We note that the non-parametric nature of our predictive distribution means that the training data must be available at test time.

3.2 Binary classification

Above we implicitly assume that the LOO posterior probability $p(y_n|\mathbf{y}_{n,k}, \mathbf{X}_{n,k}, \mathbf{x}_n)$ can be computed analytically. What if this is not the case, as happens in classification? In this section we briefly describe how we define a LOO training objective for binary classification. The basic strategy is to introduce auxiliary variables that restore Gaussianity and thus enable closed form (conditional) posterior distributions. Let $\mathcal{D} = \{(\mathbf{x}_n, y_n)\}_{n=1}^N$ with $y_n \in \{-1, 1\}$ and consider a GP classifier with likelihood $p(y_n|f(\mathbf{x}_n)) = [1 + \exp(-y_n f(\mathbf{x}_n))]^{-1}$ governed by a logistic function. We introduce a N -dimensional vector of Pòlya-Gamma [Polson et al., 2013] auxiliary variables ω and exploit the identity $[1 + e^\psi]^{-1} = \frac{1}{2} \mathbb{E}_{p(\omega|1,0)} [\exp(-\frac{1}{2}\omega\psi^2 - \frac{1}{2}\psi)]$ to massage the likelihood terms into Gaussian form and end up with a joint density proportional to

$$p(\omega)p(\mathbf{f}|\mathbf{K}_{N,N}) \exp\left(\frac{1}{2}\mathbf{y}^T\mathbf{f} - \frac{1}{2}\mathbf{f}^T\Omega\mathbf{f}\right) \quad (10)$$

where $\Omega \equiv \text{diag}(\omega)$ is a diagonal $N \times N$ matrix. Note that this augmentation is exact. We proceed to integrate out \mathbf{f} and perform variational inference w.r.t. ω . This results in the variational objective

$$\mathcal{L}_{\text{ELBO}} = \mathbb{E}_{q(\omega)} [\log p(\mathbf{y}|\mathbf{X}, \omega)] - \text{KL}(q(\omega)|p(\omega)) + \frac{1}{8} \mathbb{E}_{q(\omega)} [\Sigma_n \omega_n^{-1}] \quad (11)$$

where we take $q(\omega)$ to be a mean-field log-Normal variational distribution and KL denotes the Kullback-Leibler divergence. We then replace $\log p(\mathbf{y}|\mathbf{X}, \omega)$ with its LOO approximation to obtain

$$\mathcal{L}_{\text{LOO}} \equiv \frac{1}{N} \sum_{n=1}^N \mathbb{E}_{q(\omega)} [\log p(y_n|\mathbf{y}_{-n}, \mathbf{X}, \omega_{-n})] - \text{KL}(q(\omega)|p(\omega)) + \frac{1}{8} \mathbb{E}_{q(\omega)} [\Sigma_n \omega_n^{-1}] \quad (12)$$

where the (conditional) posterior predictive distribution $p(y_n|\mathbf{y}_{-n}, \mathbf{X}, \omega_{-n})$ is given by

$$p(y_n|\mathbf{y}_{-n}, \mathbf{X}, \omega_{-n}) \equiv \int df_n p(y_n|f_n) p(f_n|\mathbf{y}_{-n}, \mathbf{X}, \omega_{-n}) \quad (13)$$

Here the (conditional) posterior over the latent function value f_n , namely $p(f_n|\mathbf{y}_{-n}, \mathbf{X}, \omega_{-n})$, is given by the Normal distribution $\mathcal{N}(f_n|\mu_n, \sigma_n^2)$ with mean and variance equal to

$$\begin{aligned} \mu_n &= \frac{1}{2} \mathbf{K}_{-n,n}^T (\mathbf{K}_{-n,-n} + \Omega_{-n}^{-1})^{-1} \Omega_{-n}^{-1} \mathbf{y}_{-n} & \mathbf{K}_{-n,n} &\equiv K(\mathbf{X}_{-n}, \mathbf{x}_n) \in \mathbb{R}^{n-1,1} \\ \sigma_n^2 &= K_{n,n} - \mathbf{K}_{-n,n}^T (\mathbf{K}_{-n,-n} + \Omega_{-n}^{-1})^{-1} \mathbf{K}_{-n,n} & \mathbf{K}_{-n,-n} &\equiv K(\mathbf{X}_{-n}, \mathbf{X}_{-n}) \in \mathbb{R}^{n-1,n-1} \end{aligned}$$

We approximate the univariate integral in Eqn. 13 with Gauss-Hermite quadrature. Our final objective function is obtained by applying a k -nearest-neighbor truncation to Eqn. 12. To maximize this objective function we use standard techniques from stochastic variational inference, including data subsampling and reparameterized gradients of ω . At test time predictions can be obtained by computing Eqn. 13 after conditioning on a sample $\omega \sim q(\omega)$.⁷ The computational cost of a training iteration is $\mathcal{O}(Bk^3 + BQ)$, where Q is the number of points in the quadrature rule. For a more comprehensive derivation and additional details on binary classification see Sec. A.5.

3.3 Multi-class classification

The Pòlya-Gamma auxiliary variable construction used in Sec. 3.2 can be generalized to the multi-class setting with K classes using a stick-breaking construction [Linderman et al., 2015]. Among other disadvantages, this construction requires choosing a class ordering. To avoid this, and to obtain linear computational scaling in the number of classes K , we instead opt for a one-against-all construction, which results in a $\mathcal{O}(BKK^3 + BKQ)$ computational cost per training iteration. We refer the reader to Sec. A.6 for details and Sec. 5.8 for empirical results.

⁷In practice we use a single sample, since we found negligible gains from averaging over multiple samples.

3.4 Other likelihoods

The auxiliary variable construction in Sec. 3.2-3.3 can be extended to a number of other likelihoods. For example, Pòlya-Gamma auxiliary variables can also be used to accomodate binomial and negative binomial likelihoods [Polson et al., 2013]. Additionally, gamma auxiliary variables can be used to accomodate a Student’s t likelihood, which is useful for modeling heavy-tailed noise.

4 Related work

Our work is related to various research directions in machine learning and statistics. Here we limit ourselves to an abbreviated account and refer the reader to Sec. A.1 for a more detailed discussion.

Nearest neighbor constructions in the GP context have been explored by several authors. Datta et al. [2016] define a Nearest Neighbor Gaussian Process, which is a valid stochastic process, derive a custom Gibbs inference scheme, and illustrate their approach on geospatial data. Vecchia approximations [Vecchia, 1988, Katzfuss and Guinness, 2021] exploit a nearest neighbor approximation to the MLL. Both these approaches can work well in 2 or 3 dimensions but tend to struggle in higher dimensions due to the need to choose a fixed ordering of the data. Gramacy and Apley [2015] introduce a ‘Local Gaussian Process Approximation’ for regression that iteratively constructs a nearest neighbor conditioning set at test time; in contrast to our approach there is no training phase.

Cross-validation (CV) in the GP (or rather kriging) context was explored as early as 1983 by Dubrule [1983]. Bachoc [2013] compares predictive performance of GPs fit with MLL and CV and concludes that CV is more robust to model mis-specification. Smith et al. [2016] consider CV losses in the context of differentially private GPs. Recent work explores how the CV score can be efficiently computed for GP regressors [Ginsbourger and Schärer, 2021, Petit et al., 2020]. Jankowiak et al. [2020b] introduce an inducing point approach for GP regression, PPGPR, that like our approach uses a loss function that is defined in terms of the predictive distribution. Indeed our approach can be seen as a non-parametric analog of PPGPR, and Eqn. 7 provides a novel conceptual framing for that approach. Fong and Holmes [2020] explore the connection between MLL and CV in the context of model evaluation and consider a decomposition like that in Eqn. 7 specialized to the case of exchangeable data. They also advocate using a Bayesian *cumulative* leave-P-out CV score for fitting models, although the computational cost limits this approach to small datasets.

Various approaches to approximate GP inference are reviewed in Liu et al. [2020]. An early application of inducing points is described in Snelson and Ghahramani [2006], which motivated various extensions to variational inference [Titsias, 2009, Hensman et al., 2013, 2015]. Wenzel et al. [2019], Galy-Fajou et al. [2020] introduce an approximate inference scheme for binary and multi-class classification that exploits inducing points, Pòlya-Gamma auxiliary variables, and variational inference.

5 Experiments

In this section we present an empirical evaluation of GPs trained with the LOO- k objective Eqn. 9. In Sec. 5.1-5.4 we explore general characteristics of our method and in Sec. 5.5-5.8 we compare our method to a variety of baseline methods for GP regression and classification.

5.1 Model mis-specification

We explore whether the LOO- k objective in Eqn. 9 is robust to model mis-specification, as we would expect following the discussion in Sec. 3. Since models can be mis-specified in a great variety of ways, it is difficult to make quantitative statements about mis-specification in general terms. Instead we choose a simple controlled setting where we can toggle the degree of mis-specification. First we sample 8096 data points \mathbf{X} uniformly from the cube $[-1, 1]^4 \subset \mathbb{R}^4$. Next we generate targets \mathbf{y} using a GP prior specified by an isotropic stationary RBF kernel with observation noise $\sigma_{\text{obs}} = 0.1$. We then apply a coordinatewise warping to each \mathbf{x}_n , where the warping is given by the identity mapping for $x_i \geq 0$ and $x_i \rightarrow (1 + \gamma)x_i$ for $x_i < 0$. We use half the data points for training and the remainder for testing predictive performance. The results can be seen in Fig. 1. We see that as γ increases and the dataset becomes more non-stationary, the LOO- k GP exhibits superior predictive performance. We note that the degraded test log likelihood of the MLL GP for large γ stems in part from severely

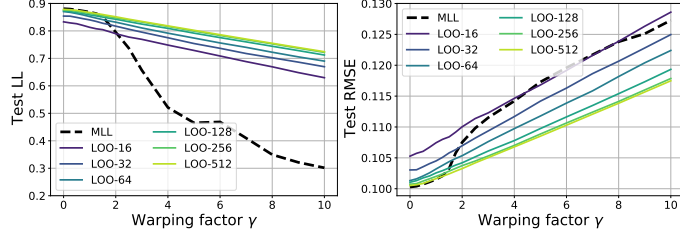


Figure 1: We compare predictive performance of a GP trained with a LOO- k objective (see Eqn. 9) to a GP trained via MLL (marginal log likelihood), where the GP regressor is mis-specified due to non-stationarity in the dataset introduced by a warping function controlled by γ . As γ increases and the dataset becomes more non-stationary, the LOO- k GP exhibits superior predictive performance, both w.r.t. log likelihood (LL) and root mean squared error (RMSE). See Sec. 5.1 for details.

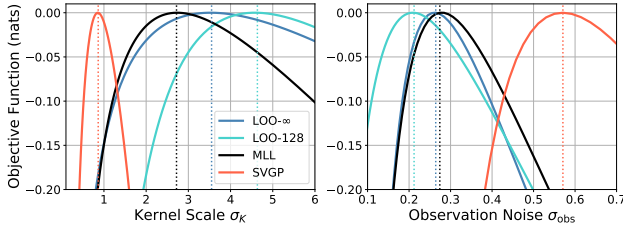


Figure 2: We depict how the objective functions for MLL, LOO- k and SVGP vary as a function of the kernel scale σ_K and the observation noise σ_{obs} for the UCI Bike dataset. To ease comparison we shift each objective function so that its maximum value is zero. σ_K and σ_{obs} are maximized at $\{3.55, 4.64, 2.72, 0.86\}$ and $\{0.26, 0.21, 0.27, 0.57\}$ for LOO- ∞ , LOO-128, MLL, and SVGP, respectively. Each objective function is normalized by the size of the training dataset N . See Sec. 5.2 for details.

underestimating the observation noise σ_{obs} . Fig. 1 confirms our expectation that using a CV-based objective can be more robust to model mis-specification, especially as the latter becomes more severe.

5.2 Objective function comparison

In Fig. 2 we compare how the MLL, SVGP, and LOO- k objective functions depend on the kernel hyperparameters σ_K and σ_{obs} . First we subsample the UCI Bike dataset to $N = 2000$ datapoints. We then train a GP using MLL on this dataset and keep all the hyperparameters fixed to their MLL values except for the one hyperparameter that is varied. Fig. 2 makes apparent the well-known tendency of SVGP to overestimate the observation noise σ_{obs} and, consequently, prefer a smaller value of σ_K [Bauer et al., 2016]. This overestimation of σ_{obs} can lead to severe overestimation of uncertainty at test time. Since σ_K and σ_{obs} appear symmetrically in Eqn. 5 and likewise in $\mathcal{L}_{\text{LOO}}^k$, the LOO- k GP does not exhibit the same tendency (as argued in [Jankowiak et al., 2020b]).

5.3 Dependence on number of nearest neighbors k

In Fig. 3 we explore how predictive performance of a LOO- k GP depends on the number of nearest neighbors k . As expected, we generally find that performance improves as k increases, although the degree of improvement depends on the particular dataset. In addition the marginal gains of increasing k past $k \sim 128$ are small on most datasets. This finding is advantageous for our method with respect to computational cost, whereas inducing point methods often require $M \gtrsim 500$ to achieve good model fit. This tendency is easy to understand, since the M inducing points need to ‘compress’ the entire dataset, while the k nearest neighbors only need to model the vicinity of a given test point.

5.4 Runtime performance

In Fig. 4 we compare the runtime performance of LOO- k to SVGP on datasets from $N = 1000$ to $N = 5$ million. As discussed further in Sec. A.3, we can take these two methods’ runtimes as

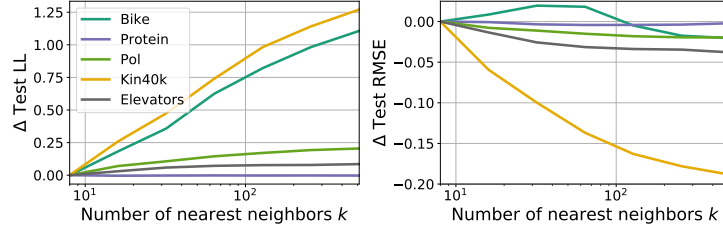


Figure 3: We depict how the predictive performance of a LOO- k GP varies w.r.t. the number of nearest neighbors k . For each of the five UCI datasets, we depict mean test log likelihood and mean RMSE averaged over 10 train/test splits. To ease comparison we shift each LL/RMSE curve so that it intersects zero at $k = 8$. See Sec. 5.3 for discussion.

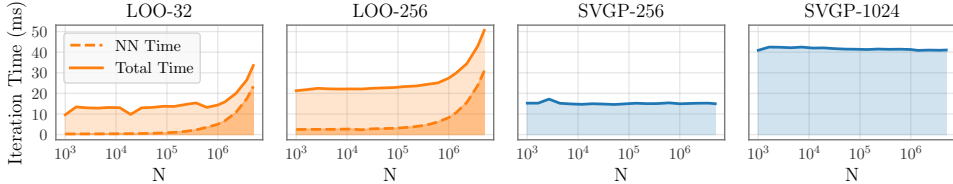


Figure 4: We compare the time per training iteration for LOO- k ($k = 32$ and $k = 256$ nearest neighbors) versus SVGP ($M = 256$ and $M = 1024$ inducing points) on a univariate regression task in $D = 25$ dimensions. Along the horizontal axis we vary the size of the training dataset N . We use a mini-batch size of 128 and run on a GeForce RTX 2080 GPU. The dotted line indicates the time spent on nearest neighbor queries; we update the nearest neighbor index every 50 gradient steps.

representative of other nearest neighbor (e.g. Vecchia) and inducing point (e.g. PPGPR) methods, respectively. Thanks to highly parallel GPU-accelerated nearest neighbor algorithms [Johnson et al., 2019], only a small fraction of LOO- k training time is devoted to nearest neighbors queries up to $N \sim 10^6$. Though these queries become more costly as N approaches 10 million, LOO- k is comparable to SVGP in this regime, and search time can be improved by sharding or other approximations. Since a LOO- k regressor is fully parameterized by a handful of kernel hyperparameters and does not make use of variational parameters, it requires substantially fewer gradient steps to converge. For example on the Kegg-undirected dataset with $N = 47706$ considered in the next section we find that LOO-256 trains ~ 4 x faster than SVGP with $M = 1024$ inducing points.

5.5 Univariate regression

We compare the performance of GP regressors trained with the LOO- k objective in Eqn. 9 to five scalable baseline methods. SVGP [Hensman et al., 2013] and PPGPR [Jankowiak et al., 2020b] are both inducing point methods; SVGP targets the MLL via an ELBO lower bound, while PPGPR uses a regularized cross-validation loss. The remaining baselines, MLL- k , Vecchia, and ALC, exploit nearest neighbors. MLL- k uses a biased k -nearest-neighbor truncation of the MLL for training [Chen et al., 2020]. Vecchia [Vecchia, 1988] uses a different k -nearest-neighbor approximation of the MLL that requires specifying a fixed ordering of the data. ALC [Gramacy and Apley, 2015] iteratively constructs a nearest neighbor conditioning set at test time using a variance reduction criterion and chooses hyperparameters using the ‘local’ MLL. See Sec. A.2 in the supplemental materials for a conceptual framing of these different approaches. We also include a comparison to GPs trained with MLL using the methodology in Wang et al. [2019]. See Sec. A.7 for additional experimental details.

The results are depicted in Fig. 5 and summarized in Table 1. We find that LOO- k exhibits the best predictive performance overall, both w.r.t. log likelihood and RMSE, followed by MLL- k . ALC performs well on some datasets but poorly on others; indeed we are unable to obtain reasonable results on the Kegg-directed dataset. Vecchia does poorly overall, presumably due to the need to use a strict ordering of the data. SVGP also does poorly overall; as argued by Bauer et al. [2016] and Jankowiak et al. [2020b] degraded performance w.r.t. log likelihood can be traced to a tendency to overestimate the observation noise and consequently underestimate function uncertainty. PPGPR exhibits good log likelihoods but poor RMSE performance due to the priority it places on uncertainty

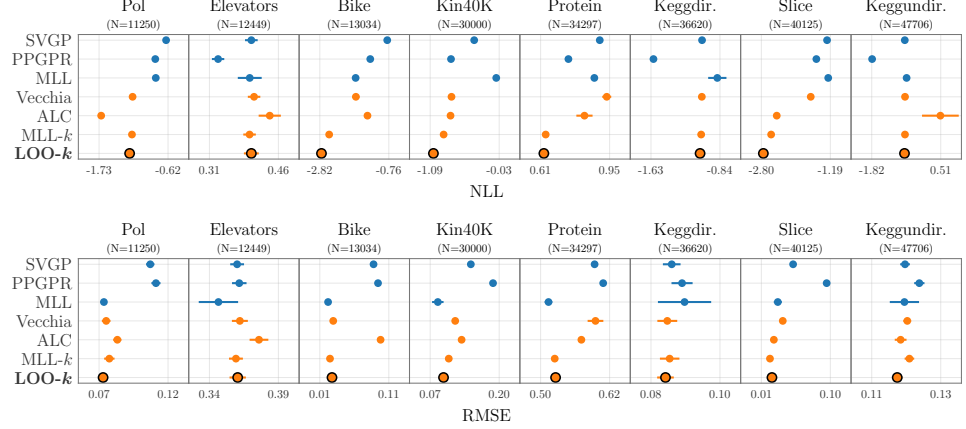


Figure 5: We depict predictive negative log likelihoods (NLL, top) and root mean squared error (RMSE, bottom) for 8 univariate regression datasets, comparing LOO- k to six baseline methods. Results are averaged over 10 dataset splits. Lower numbers are better. Methods in orange utilize nearest neighbors. Here and elsewhere horizontal bars denote standard errors. Results for SVGP, PPGPR, and MLL are reproduced from [Jankowiak et al., 2020b].

	SVGP	PPGPR	Vecchia	ALC	MLL- k	LOO- k
NLL	4.92	3.15	4.30	4.05	2.58	2.00
RMSE	3.92	5.42	3.21	4.17	2.31	1.95
CRPS	5.12	3.46	4.19	3.62	2.60	2.00

Table 1: We summarize the performance ranking of various GP methods on the univariate regression experiments in Figure 5 averaged over all dataset splits. CRPS is the Continuous Ranking Probability Score [Gneiting and Raftery, 2007]. Lower is better for all metrics.

quantification. It is also worth highlighting that the nearest neighbor methods can perform well in high-dimensional input spaces; e.g. the Slice dataset is 380-dimensional.

5.6 Multivariate regression

We continue our empirical evaluation by considering four multivariate regression datasets. In each dataset the input and output dimensions correspond to various joint positions/velocities/etc. of a robot. Each GP regressor employs the structure of the so-called linear model of coregionalization (LMC) [Alvarez et al., 2012]. We compare against three baseline methods: SVGP, PPGPR, and MLL- k . The results are depicted in Fig. 6 and summarized in Table 2. We find that the two nearest neighbor methods, LOO- k and MLL- k , outperform the two inducing point methods, SVGP and PPGPR, with LOO- k and MLL- k performing the best w.r.t. NLL and RMSE, respectively. Strikingly, for 3/4 datasets the RMSEs for the nearest neighbor methods are much smaller than for the inducing point methods, even though we use no more than $k = 32$ nearest neighbors. We hypothesize that it is difficult to capture the complex non-linear dynamics underlying these datasets using a limited number of inducing points. In addition, training objectives that depend on large numbers of inducing points can be challenging to optimize, potentially resulting in suboptimal solutions. This highlights one of the advantages of methods like LOO- k and MLL- k , which avoid optimization in input space and result in flexible non-parametric nearest neighbor predictive distributions.

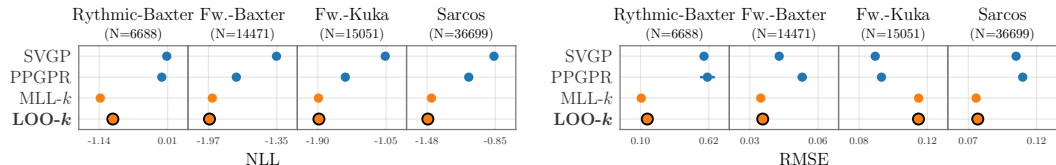


Figure 6: We depict predictive negative log likelihoods (NLL, left) and root mean squared error (RMSE, right) for 4 multivariate regression datasets. Results are averaged over 10 dataset splits. Lower numbers are better. Results for SVGP and PPGPR are from [Jankowiak et al., 2020a].

Table 2: We summarize the performance ranking of various GP methods on the multivariate regression experiments in Fig. 6 averaged over all dataset splits.

Table 3: We summarize the performance ranking of various GP methods for binary classification averaged over all dataset splits. Lower is better for both metrics.

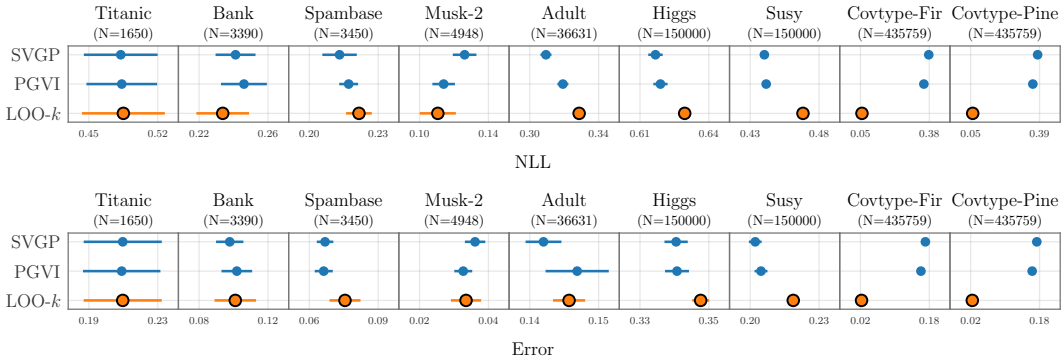


Figure 7: We depict predictive negative log likelihood (NLL, top) and error (bottom) for 9 binary classification datasets. Results are averaged over 5 dataset splits. Lower numbers are better.

5.7 Binary classification

Next we compare the predictive performance of the LOO- k objective for binary classification, Eqn. 12, to two scalable GP baselines. Both SVGP [Hensman et al., 2015] and PGVI [Wenzel et al., 2019] are inducing point methods that utilize variational inference; PGVI also makes use of natural gradients and Pòlya-Gamma augmentation. The results are depicted in Fig. 7 and summarized in Table 3. The predictive performance is broadly comparable for most datasets. Most striking is the superior performance of LOO- k on the two Covtype datasets, which exhibit (geospatial) decision boundaries with complex topologies that are difficult to capture with a limited number of inducing points.

5.8 Multi-class classification

We compare the predictive performance of the LOO- k objective for multi-class classification to a SVGP baseline. See Sec. A.6 for more details on the method. We consider thirteen datasets with five splits per dataset for a total of 65 splits. We find that LOO- k outperforms SVGP on 41/65 and 42/65 splits w.r.t. log likelihood and error rate, respectively. See Sec. A.8 for complete results.

6 Discussion

Most scalable methods for fitting Gaussian process models target the marginal log likelihood. As we have shown, the fusion of cross-validation and nearest neighbor truncation provides an alternative path to scalability. The resulting method is simple to implement and offers fast training and excellent predictive performance, both for regression and classification. We note two limitations of our approach. First, non-Gaussian likelihoods that do not admit suitable auxiliary variables may be difficult to accommodate. Second, nearest neighbor queries may be prohibitively slow for datasets with tens of millions of data points. Modifications to our basic approach may be required to support this regime, including for example approximate nearest neighbor queries or dataset sharding.

An open question is whether neural networks can be effectively incorporated into LOO- k GPs, whether into the mean or covariance function. In the latter case, nearest neighbor queries would be performed on a learned feature representation that evolves throughout training, which may make it more difficult to perform queries efficiently. In any case, combining the flexibility of neural networks with the non-parametric uncertainty quantification offered by nearest neighbor GPs is an attractive direction for future work.

References

Mauricio A Alvarez, Lorenzo Rosasco, Neil D Lawrence, et al. Kernels for vector-valued functions: A review. *Foundations and Trends® in Machine Learning*, 4(3):195–266, 2012.

François Bachoc. Cross validation and maximum likelihood estimations of hyper-parameters of gaussian processes with model misspecification. *Computational Statistics & Data Analysis*, 66: 55–69, 2013.

Jarred Barber. Sparse gaussian processes via parametric families of compactly-supported kernels. *arXiv preprint arXiv:2006.03673*, 2020.

Matthias Bauer, Mark van der Wilk, and Carl Edward Rasmussen. Understanding probabilistic sparse gaussian process approximations. In *Advances in neural information processing systems*, pages 1533–1541, 2016.

Jon Louis Bentley. Multidimensional binary search trees used for associative searching. *Communications of the ACM*, 18(9):509–517, 1975.

Eli Bingham, Jonathan P. Chen, Martin Jankowiak, Fritz Obermeyer, Neeraj Pradhan, Theofanis Karaletsos, Rohit Singh, Paul A. Szerlip, Paul Horsfall, and Noah D. Goodman. Pyro: Deep universal probabilistic programming. *J. Mach. Learn. Res.*, 20:28:1–28:6, 2019. URL <http://jmlr.org/papers/v20/18-403.html>.

Hao Chen, Lili Zheng, Raed Al Kontar, and Garvesh Raskutti. Stochastic gradient descent in correlated settings: A study on gaussian processes. *Advances in Neural Information Processing Systems*, 33, 2020.

Abhirup Datta, Sudipto Banerjee, Andrew O Finley, and Alan E Gelfand. Hierarchical nearest-neighbor gaussian process models for large geostatistical datasets. *Journal of the American Statistical Association*, 111(514):800–812, 2016.

Dheeru Dua and Casey Graff. UCI machine learning repository, 2017. URL <http://archive.ics.uci.edu/ml>.

Olivier Dubrule. Cross validation of kriging in a unique neighborhood. *Journal of the International Association for Mathematical Geology*, 15(6):687–699, 1983.

Xavier Emery. The kriging update equations and their application to the selection of neighboring data. *Computational Geosciences*, 13(3):269–280, 2009.

Edwin Fong and CC Holmes. On the marginal likelihood and cross-validation. *Biometrika*, 107(2): 489–496, 2020.

Théo Galy-Fajou, Florian Wenzel, Christian Donner, and Manfred Opper. Multi-class gaussian process classification made conjugate: Efficient inference via data augmentation. In *Uncertainty in Artificial Intelligence*, pages 755–765. PMLR, 2020.

David Ginsbourger and Cedric Schärer. Fast calculation of gaussian process multiple-fold cross-validation residuals and their covariances. *arXiv preprint arXiv:2101.03108*, 2021.

Tilmann Gneiting and Adrian E Raftery. Strictly proper scoring rules, prediction, and estimation. *Journal of the American statistical Association*, 102(477):359–378, 2007.

Robert B Gramacy. lags: Large-scale spatial modeling via local approximate gaussian processes in r. *Journal of Statistical Software*, 72(1):1–46, 2016.

Robert B Gramacy and Daniel W Apley. Local gaussian process approximation for large computer experiments. *Journal of Computational and Graphical Statistics*, 24(2):561–578, 2015.

James Hensman, Nicolo Fusi, and Neil D Lawrence. Gaussian processes for big data. *arXiv preprint arXiv:1309.6835*, 2013.

James Hensman, Alexander Matthews, and Zoubin Ghahramani. Scalable variational gaussian process classification. 2015.

Martin Jankowiak, Geoff Pleiss, and Jacob Gardner. Deep sigma point processes. In *Conference on Uncertainty in Artificial Intelligence*, pages 789–798. PMLR, 2020a.

Martin Jankowiak, Geoff Pleiss, and Jacob Gardner. Parametric gaussian process regressors. In *International Conference on Machine Learning*, pages 4702–4712. PMLR, 2020b.

Jeff Johnson, Matthijs Douze, and Hervé Jégou. Billion-scale similarity search with gpus. *IEEE Transactions on Big Data*, 2019.

Matthias Katzfuss and Joseph Guinness. A general framework for vecchia approximations of gaussian processes. *Statistical Science*, 36(1):124–141, 2021.

Diederik P Kingma and Jimmy Ba. Adam: A method for stochastic optimization. *arXiv preprint arXiv:1412.6980*, 2014.

Loic Le Gratiet and Claire Cannamela. Cokriging-based sequential design strategies using fast cross-validation techniques for multi-fidelity computer codes. *Technometrics*, 57(3):418–427, 2015.

Scott W Linderman, Matthew J Johnson, and Ryan P Adams. Dependent multinomial models made easy: Stick breaking with the p\'olya-gamma augmentation. *arXiv preprint arXiv:1506.05843*, 2015.

Haitao Liu, Yew-Soon Ong, Xiaobo Shen, and Jianfei Cai. When gaussian process meets big data: A review of scalable gps. *IEEE Transactions on Neural Networks and Learning Systems*, 2020.

Andrés R Masegosa. Learning under model misspecification: Applications to variational and ensemble methods. *arXiv preprint arXiv:1912.08335*, 2019.

Arman Melkumyan and Fabio Ramos. A sparse covariance function for exact gaussian process inference in large datasets. In *IJCAI*, volume 9, pages 1936–1942, 2009.

Sébastien Petit, Julien Bect, Sébastien Da Veiga, Paul Feliot, and Emmanuel Vazquez. Towards new cross-validation-based estimators for gaussian process regression: efficient adjoint computation of gradients. *arXiv preprint arXiv:2002.11543*, 2020.

Nicholas G Polson, James G Scott, and Jesse Windle. Bayesian inference for logistic models using p\'olya-gamma latent variables. *Journal of the American statistical Association*, 108(504):1339–1349, 2013.

Carl Edward Rasmussen. Gaussian processes in machine learning. In *Summer School on Machine Learning*, pages 63–71. Springer, 2003.

Rishit Sheth and Roni Kharon. Pseudo-bayesian learning via direct loss minimization with applications to sparse gaussian process models. In *Symposium on Advances in Approximate Bayesian Inference*, pages 1–18. PMLR, 2020.

Michael Thomas Smith, Max Zwiessele, and Neil D Lawrence. Differentially private gaussian processes. *arXiv preprint arXiv:1606.00720*, 2016.

Edward Snelson and Zoubin Ghahramani. Sparse gaussian processes using pseudo-inputs. In *Advances in neural information processing systems*, pages 1257–1264, 2006.

Michalis Titsias. Variational learning of inducing variables in sparse gaussian processes. In *Artificial Intelligence and Statistics*, pages 567–574, 2009.

Aldo V Vecchia. Estimation and model identification for continuous spatial processes. *Journal of the Royal Statistical Society: Series B (Methodological)*, 50(2):297–312, 1988.

Ke Wang, Geoff Pleiss, Jacob Gardner, Stephen Tyree, Kilian Q Weinberger, and Andrew Gordon Wilson. Exact gaussian processes on a million data points. In *Advances in Neural Information Processing Systems*, pages 14648–14659, 2019.

Yadi Wei, Rishit Sheth, and Roni Khardon. Direct loss minimization for sparse gaussian processes. In *International Conference on Artificial Intelligence and Statistics*, pages 2566–2574. PMLR, 2021.

Florian Wenzel, Théo Galy-Fajou, Christian Donner, Marius Kloft, and Manfred Opper. Efficient gaussian process classification using pôlya-gamma data augmentation. In *Proceedings of the AAAI Conference on Artificial Intelligence*, volume 33, pages 5417–5424, 2019.

Hao Zhang and Yong Wang. Kriging and cross-validation for massive spatial data. *Environmetrics: The official journal of the International Environmetrics Society*, 21(3-4):290–304, 2010.

A Appendix

Algorithm 1: We outline the main steps in learning a LOO- k GP in the case of univariate regression.

Input: Dataset $\mathcal{D} = (\mathbf{y}, \mathbf{X})$ with N data points; number of nearest neighbors k ; optimizer `optim`; mini-batch size B ; number of iterations T ; nearest neighbor index update frequency T_{nn} ; initial kernel hyperparameters $\{\rho_i^0, \sigma_K^0, \sigma_{obs}^0\}$

Output: Learned kernel hyperparameters $\{\rho_i^T, \sigma_K^T, \sigma_{obs}^T\}$

- 1 **for** $t = 1, \dots, T$ **do**
- 2 If $t - 1 = 0 \bmod T_{nn}$ (re)compute the nearest neighbor index using $\{\rho_i^{t-1}\}$
- 3 Choose a random mini-batch of indices of size B : $\mathcal{I} \subset \{1, \dots, N\}$ with $|\mathcal{I}| = B$
- 4 For each $i \in \mathcal{I}$ form the k -nearest-neighbor tuple $(\mathbf{y}_{i,k}, \mathbf{X}_{i,k})$
- 5 Compute a stochastic estimate $\hat{\mathcal{L}}_{\text{LOO}}^k$ of Eqn. 9 using Eqn. 4-5, $\{(\mathbf{y}_{i,k}, \mathbf{X}_{i,k})\}_{i=1}^B$ and $\{\rho_i^{t-1}, \sigma_K^{t-1}, \sigma_{obs}^{t-1}\}$
- 6 Let $\{\rho_i^t, \sigma_K^t, \sigma_{obs}^t\} = \text{optim}(\hat{\mathcal{L}}_{\text{LOO}}^k)$
- 7 **return** $\{\rho_i^T, \sigma_K^T, \sigma_{obs}^T\}$

A.1 Related work (extended)

Nearest neighbor constructions in the GP context have been explored by several authors. Vecchia approximations [Vecchia, 1988, Katzfuss and Guinness, 2021] exploit a nearest neighbor approximation to the MLL. This approach can work well in 2 or 3 dimensions but tends to struggle in higher dimensions due to the need to choose a fixed ordering of the data. Datta et al. [2016] extend the Vecchia approach to the Nearest Neighbor Gaussian Process, which is a valid stochastic process, deriving a custom Gibbs inference scheme, and illustrating their approach on geospatial data. Chen et al. [2020] explore a different biased approximation to the MLL, which does not require specifying an ordering of the data and which we refer to as MLL- k . For more details on Vecchia approximations and MLL- k see the next section, Sec. A.2. Gramacy and Apley [2015], Gramacy [2016], addressing the computer simulation community, introduce a ‘Local Gaussian Process Approximation’ for regression that iteratively constructs a nearest neighbor conditioning set at test time; in contrast to our approach there is no training phase. Somewhat related to nearest neighbors, several authors have explored the computational advantages of compactly-supported kernels [Melkumyan and Ramos, 2009, Barber, 2020].

Cross-validation (CV) in the GP (or rather kriging) context was explored as early as 1983 by Dubrule [1983], with follow-up work including Emery [2009], Zhang and Wang [2010], and Le Gratiet and Cannamela [2015]. Bachoc [2013] compares predictive performance of GPs fit with MLL and CV and concludes that CV is more robust to model mis-specification. The classic GP textbook Rasmussen [2003] also briefly touches on CV in the GP setting. Smith et al. [2016] consider CV losses in the context of differentially private GPs. Recent work explores how the CV score can be efficiently computed for GP regressors [Ginsbourger and Schärer, 2021, Petit et al., 2020]. Jankowiak et al. [2020b] introduce an inducing point approach for GP regression, PPGPR, that like our approach uses a loss function that is defined in terms of the predictive distribution. Indeed our approach can be seen as a non-parametric analog of PPGPR, and Eqn. 7 provides a novel conceptual framing for

Method	Targets MLL?	Targets CV?	Inducing Points?	Nearest Neighbors?	Notes
SVGP	✓	✗	✓	✗	Variational lower bound to MLL
PPGPR	✗	✓	✓	✗	CV loss includes additional regularizers
MLL- k	✓	✗	✗	✓	Does not require fixed dataset ordering
Vecchia	✓	✗	✗	✓	Requires fixed dataset ordering
ALC	✓	✗	✗	✓	No training phase
LOO- k	✗	✓	✗	✓	

Table 4: We summarize the conceptual differences between six of the methods for GP regression benchmarked in Sec. 5.5.

that approach. PPGPR and LOO- k are also related to Direct Loss Minimization, which emerges from a view of approximate inference as regularized loss minimization [Sheth and Kharden, 2020, Wei et al., 2021]. Fong and Holmes [2020] explore the connection between MLL and CV in the context of model evaluation and consider a decomposition like that in Eqn. 7 specialized to the case of exchangeable data. They also advocate using a Bayesian *cumulative* leave- P -out CV score for fitting models, although the computational cost limits this approach to small datasets.

Various approaches to approximate GP inference are reviewed in Liu et al. [2020]. An early application of inducing points is described in Snelson and Ghahramani [2006], which motivated various extensions to variational inference [Titsias, 2009, Hensman et al., 2013, 2015]. Wenzel et al. [2019], Galy-Fajou et al. [2020] introduce an approximate inference scheme for binary and multi-class classification that exploits inducing points, Pólya-Gamma auxiliary variables, and variational inference.

A.2 Objective function summary

In Table 4 we provide a conceptual summary of how the different methods for scalable GP regression benchmarked in Sec. 5.5 are formulated. We note that Vecchia and MLL- k are quite similar, as both utilize nearest neighbor truncation to target the MLL. The Vecchia approximation does this using a fixed ordering in a decomposition of the MLL into a product of univariate conditionals, while MLL- k ignores the restrictions that are imposed by a specific ordering. Both approximations result in biased approximations of the MLL, and for both methods we utilize mini-batch training. In particular for Vecchia the objective function is of the form

$$\mathcal{L}_{\text{Vecchia}} = \frac{1}{N} \sum_{n=1}^N \log p(y_n | \mathbf{X}_{n,k}^{\text{Vecchia}}, \mathbf{y}_{n,k}^{\text{Vecchia}}, \mathbf{x}_n) \quad (14)$$

where $\mathbf{X}_{n,k}^{\text{Vecchia}}$ and $\mathbf{y}_{n,k}^{\text{Vecchia}}$ are the k nearest neighbors of \mathbf{x}_n that respect a given ordering of the data. For example, for $n' \geq n$ we necessarily have that $y_{n'} \notin \mathbf{y}_{n,k}$. Since the Vecchia approximation respects a fixed ordering of a data, it can be understood as a nearest neighbor approximation to a particular decomposition of the MLL. Conversely for MLL- k the objective function takes the form

$$\mathcal{L}_{\text{MLL}}^k = \frac{1}{N} \sum_{n=1}^N \log p(y_{n,k}^{\text{MLL}} | \mathbf{X}_{n,k}^{\text{MLL}}) \quad (15)$$

where, for example, $\mathbf{X}_{n,k}^{\text{MLL}}$ consists of the $k - 1$ nearest neighbors of \mathbf{x}_n together with \mathbf{x}_n itself.

A.3 Computational complexity

We provide a brief discussion of the computational complexity of LOO- k as compared to other scalable GP methods. For simplicity we limit our discussion to the case of univariate regression. Let M be the number of inducing points, k be the number of nearest neighbors, and B be the size of the mini-batch. The computational complexity of SVGP and PPGPR are identical. In particular the time complexity of a training step is $\mathcal{O}(BM^2 + M^3)$ and the space complexity is $\mathcal{O}(M^2 + BM)$, while the time and space complexity at test time (for a single input) are both $\mathcal{O}(M^2)$. The computational complexity of Vecchia, MLL- k , and LOO- k are identical. During training, we must compute the set of k -nearest neighbors for each training data point, which takes $\mathcal{O}(N \log N)$ time (or $\mathcal{O}(N^2)$ time with a brute-force approach). Once the nearest neighbors are computed, the time complexity of a training step is $\mathcal{O}(Bk^3)$ and the space complexity is $\mathcal{O}(Bk^2)$. During testing, the time and space

complexity (for a single input) are $\mathcal{O}(\log N + k^3)$ and $\mathcal{O}(k^2)$, respectively. The $\mathcal{O}(\log N)$ factor is the time to compute the test input's nearest neighbors ($\mathcal{O}(N)$ with a brute-force approach), and the $\mathcal{O}(k^3)$ factor is the cost of computing the posterior mean and variance.

A.4 Pòlya-Gamma density

The probability density function of the Pòlya-Gamma distribution $p(\omega|1,0)$, which has support on the positive real line, is given by the alternating series [Polson et al., 2013]:

$$p(\omega|1,0) = \sum_{n=0}^{\infty} (-1)^n \frac{2n+1}{\sqrt{2\pi\omega^3}} \exp(-(2n+1)^2/8\omega) \quad (16)$$

The mean of this distribution is given by $\frac{1}{4}$ and the vast majority of the probability mass is located in the interval $\omega \in (0, 2.5)$. To perform variational inference w.r.t. $p(\omega|1,0)$ we need to be able to compute this density. We leverage the implementation in Pyro [Bingham et al., 2019], which is formulated as follows. Estimating Eqn. 16 accurately requires computing increasingly many terms in the alternating sum as ω increases. To address this issue we truncate the distribution to the interval $(0, 2.5)$. We then retain the leading 7 terms in Eqn. 16. This is accurate to about 6 decimal places over the entire truncated domain. We find that this approximation is sufficient for our purposes. We note that as a consequence of the truncation our variational distribution is properly speaking a truncated log-Normal distribution, although given the large truncation point and given that most of the posterior mass concentrates in $\omega \in (0, 0.5)$ the truncation of $q(\omega)$ plays a negligible role numerically and can be safely ignored.

A.5 Binary classification

We expand on our method for binary GP classification discussed in Sec. 3.2. We consider a dataset $\mathcal{D} = \{(\mathbf{x}_n, y_n)\}_{n=1}^N$ with $y_n \in \{-1, 1\}$ and a GP with joint density given by

$$p(\mathbf{f}|\mathbf{K}_{N,N}) \prod_{n=1}^N p(y_n|f(\mathbf{x}_n)) \quad (17)$$

where $p(\mathbf{f}|\mathbf{K}_{N,N})$ is the GP prior, and $p(y_n|f(\mathbf{x}_n)) = [1 + \exp(-y_n f(\mathbf{x}_n))]^{-1}$ is a Bernoulli probability governed by a logistic link function. We introduce a N -dimensional vector of Pòlya-Gamma auxiliary variables $\boldsymbol{\omega}$ and exploit the identity [Polson et al., 2013]

$$\frac{e^\psi}{1 + e^\psi} = \frac{1}{2} e^{\frac{1}{2}\psi} \mathbb{E}_{p(\omega|1,0)} \left[e^{-\frac{1}{2}\omega\psi^2} \right] \quad (18)$$

and the shorthand $f_n = f(\mathbf{x}_n)$ to write

$$\prod_{n=1}^N p(y_n|f_n) = \prod_{n=1}^N \frac{1}{1 + \exp(-y_n f_n)} = \prod_{n=1}^N \frac{\exp(y_n f_n)}{1 + \exp(y_n f_n)} \quad (19)$$

$$= 2^{-N} \prod_{n=1}^N \mathbb{E}_{p(\omega_n|1,0)} \left[\exp\left(\frac{1}{2}y_n f_n - \frac{1}{2}\omega_n y_n^2 f_n^2\right) \right] \quad (20)$$

$$\propto \prod_{n=1}^N \mathbb{E}_{p(\omega_n|1,0)} \left[\exp\left(\frac{1}{2}y_n f_n - \frac{1}{2}\omega_n y_n^2 f_n^2\right) \right] \propto \mathbb{E}_{p(\boldsymbol{\omega})} \left[\prod_{n=1}^N \exp\left(\frac{1}{2}\mathbf{y}^T \mathbf{f} - \frac{1}{2}\mathbf{f}^T \boldsymbol{\Omega} \mathbf{f}\right) \right] \quad (21)$$

where $\boldsymbol{\Omega} \equiv \text{diag}(\boldsymbol{\omega})$ is a diagonal $N \times N$ matrix. Crucially, thanks to the Pòlya-Gamma augmentation \mathbf{f} is now conditionally gaussian when we condition on \mathbf{y} and $\boldsymbol{\omega}$. We emphasize that this augmentation is exact. Next we integrate out \mathbf{f} . This is made easy if we recycle familiar formulae from the GP regression case. In particular write

$$\frac{1}{2}\mathbf{y}^T \mathbf{f} - \frac{1}{2}\mathbf{f}^T \boldsymbol{\Omega} \mathbf{f} = -\frac{1}{2} \sum_n \omega_n \left(f_n - \frac{y_n}{2\omega_n} \right)^2 + \sum_n \frac{1}{8\omega_n} \quad (22)$$

and observe that (apart from the last term which is independent of \mathbf{f}) this takes the form of a Normal likelihood with ‘pseudo-observations’ $\frac{y_n}{2\omega_n}$ and data point dependent observation variances ω_n^{-1} . From this we can immediately write down the marginal log likelihood:

$$\log p(\mathbf{y}|\mathbf{X}) = \log \mathbb{E}_{p(\boldsymbol{\omega})} p(\mathbf{y}|\mathbf{X}, \boldsymbol{\omega}) \quad \text{with} \quad (23)$$

$$p(\mathbf{y}|\mathbf{X}, \boldsymbol{\omega}) = \mathcal{N}\left(\frac{1}{2}\boldsymbol{\Omega}^{-1}\mathbf{y}, \mathbf{K}_{N,N} + \boldsymbol{\Omega}^{-1}\right) \times \exp\left(\sum_n \frac{1}{8\omega_n}\right) \quad (24)$$

Next we introduce a variational distribution $q(\boldsymbol{\omega})$ and apply Jensen’s inequality to obtain

$$\log p(\mathbf{y}|\mathbf{X}) \geq \mathbb{E}_{q(\boldsymbol{\omega})} [\log p(\mathbf{y}|\mathbf{X}, \boldsymbol{\omega})] - \text{KL}(q(\boldsymbol{\omega})|p(\boldsymbol{\omega})) + \frac{1}{8}\mathbb{E}_{q(\boldsymbol{\omega})} [\sum_n \omega_n^{-1}] \quad (25)$$

where we choose $q(\boldsymbol{\omega})$ to be a (truncated) mean-field log-Normal distribution. We note that if $q(\boldsymbol{\omega})$ is parameterized with location and scale parameters m and s then $\mathbb{E}_{q(\boldsymbol{\omega})} [\omega^{-1}] = \exp(-m + \frac{1}{2}s^2)$. Next we replace $\log p(\mathbf{y}|\mathbf{X}, \boldsymbol{\omega})$ with its leave-one-out approximation to obtain an objective

$$\mathcal{L}_{\text{LOO}} = \frac{1}{N} \sum_{n=1}^N \mathbb{E}_{q(\boldsymbol{\omega})} [\log p(y_n|\mathbf{y}_{-n}, \mathbf{X}, \boldsymbol{\omega}_{-n})] - \text{KL}(q(\boldsymbol{\omega})|p(\boldsymbol{\omega})) + \frac{1}{8}\mathbb{E}_{q(\boldsymbol{\omega})} [\sum_n \omega_n^{-1}] \quad (26)$$

where the (conditional) posterior predictive distribution $p(y_n|\mathbf{y}_{-n}, \mathbf{X}, \boldsymbol{\omega}_{-n})$ is given by

$$p(y_n|\mathbf{y}_{-n}, \mathbf{X}, \boldsymbol{\omega}_{-n}) \equiv \int df_n p(y_n|f_n) p(f_n|\mathbf{y}_{-n}, \mathbf{X}, \boldsymbol{\omega}_{-n}) \quad (27)$$

and where the posterior over the latent function value f_n , namely $p(f_n|\mathbf{y}_{-n}, \mathbf{X}, \boldsymbol{\omega}_{-n})$, is given by the Normal distribution $\mathcal{N}(f_n|\mu_n, \sigma_n^2)$ with mean and variance equal to

$$\mu_n = \frac{1}{2}\mathbf{K}_{-n,n}^T (\mathbf{K}_{-n,-n} + \boldsymbol{\Omega}_{-n}^{-1})^{-1} \boldsymbol{\Omega}_{-n}^{-1} \mathbf{y}_{-n} \quad (28)$$

$$\sigma_n^2 = K_{n,n} - \mathbf{K}_{-n,n}^T (\mathbf{K}_{-n,-n} + \boldsymbol{\Omega}_{-n}^{-1})^{-1} \mathbf{K}_{-n,n} \quad (29)$$

where $\boldsymbol{\Omega}_{-n}$ is the $(N-1) \times (N-1)$ diagonal matrix that omits ω_n and

$$\mathbf{K}_{-n,-n} \equiv K(\mathbf{X}_{-n}, \mathbf{X}_{-n}) \in \mathbb{R}^{n-1, n-1} \quad (30)$$

$$\mathbf{K}_{n,n} \equiv K(\mathbf{X}_{-n}, x_n) \in \mathbb{R}^{n-1, 1} \quad K_{n,n} \equiv K(x_n, x_n) \quad (31)$$

To obtain our final objective function we apply a k -nearest-neighbor truncation to Eqn. 26-31. For example this means that for each n the expression for the predictive distribution $p(y_n|\mathbf{y}_{-n}, \mathbf{X}, \boldsymbol{\omega}_{-n})$ will be replaced by an expression that only depends on the k Pòlya-Gamma variates that correspond to its nearest neighbors. We numerically approximate the univariate integral in Eqn. 27 with Gauss-Hermite quadrature using Q quadrature points.

To maximize this objective function we use standard techniques from stochastic variational inference, including data subsampling and reparameterized gradients of $\boldsymbol{\omega}$. At test time predictions can be obtained by computing Eqn. 27 after conditioning on a sample $\boldsymbol{\omega} \sim q(\boldsymbol{\omega})$. In practice we use a single sample, since we found negligible gains from averaging over multiple samples. The computational cost of a training iteration is $\mathcal{O}(Bk^3 + BQ)$, where B is the mini-batch size. Note that (excluding the cost of finding the nearest neighbors) the cost at test time for a batch of test points of size B is also $\mathcal{O}(Bk^3 + BQ)$, since the main cost of computing the objective function goes into computing the predictive distribution. In practice we take $Q = 16$ so that the cost of Gauss-Hermite quadrature is negligible. Consequently the main determinants of computational cost are B and k .

A.6 Multi-class classification

We are given a dataset $\mathcal{D} = \{(\mathbf{x}_n, \mathbf{y}_n)\}$, where each \mathbf{y}_n encodes one of K discrete labels and we suppose that \mathbf{y}_n is represented as a one-against-all encoding where $\mathbf{y}_n \in \{-1, 1\}^K$ and $y_{n,k} = 1$ for exactly one of $k \in \{1, \dots, K\}$. In the following we will effectively learn K one-against-all GP classifiers constructed as in Sec. A.5, with the difference that we will aggregate the K one-against-all classification probabilities and form a single multi-class likelihood.

In more detail we introduce a $N \times K$ matrix of Pòlya-Gamma auxiliary variables $\boldsymbol{\omega}_{n,k}$. As in Eqn. 13 for each data point n we can form K Bernoulli distributions

$$\tilde{p}(y_{n,k}|\mathbf{y}_{-n,k}, \mathbf{X}, \boldsymbol{\omega}_{-n,k}) \equiv \int df_{n,k} p(y_{n,k}|f_{n,k}) p(f_{n,k}|\mathbf{y}_{-n,k}, \mathbf{X}, \boldsymbol{\omega}_{-n,k}) \quad (32)$$

where each of the K univariate integrals can be numerically approximated with Gauss-Hermite quadrature. We use a tilde in Eqn. 32 to indicate that $\tilde{p}(y_{n,k}|\cdot)$ is an intermediate quantity that serves as an ingredient in computing a joint predictive distribution. In particular we form a joint predictive distribution by jointly normalizing all of the Bernoulli probabilities:

$$p(y_{n,k} = 1|\mathbf{y}_{-n}, \mathbf{X}, \boldsymbol{\omega}_{-n}) = \frac{\tilde{p}(y_{n,k} = 1|\cdot)}{\sum_{k'} \tilde{p}(y_{n,k'} = 1|\cdot)} \quad (33)$$

Given the matrix of Pólya-Gamma variates $\boldsymbol{\omega}_{n,k}$, $p(y_{n,k} = 1|\cdot)$ in Eqn. 33 is a normalized distribution over the label $k \in \{1, \dots, K\}$ that can be computed in closed form thanks to Gauss-Hermite quadrature. To train the kernel hyperparameters and Pólya-Gamma mean-field variational distribution we use an objective function that is a direct generalization of Eqn. 12:

$$\mathcal{L}_{\text{LOO}}^{\text{multi}} = \frac{1}{N} \sum_{n=1}^N \mathbb{E}_{q(\boldsymbol{\omega})} [\log p(y_{n,k}|\mathbf{y}_{-n}, \mathbf{X}, \boldsymbol{\omega}_{-n})] - \text{KL}(q(\boldsymbol{\omega})||p(\boldsymbol{\omega})) + \frac{1}{8} \mathbb{E}_{q(\boldsymbol{\omega})} \left[\sum_{n,k} \omega_{n,k}^{-1} \right] \quad (34)$$

The final objective function is obtained by applying a k -nearest-neighbors truncation to Eqn. 34. During test time we sample $\boldsymbol{\omega} \sim q(\boldsymbol{\omega})$ and use Eqn. 33.

A.7 Experimental details

All the datasets we use, apart from those used in the multivariate regression experiments, can be obtained from the UCI depository [Dua and Graff, 2017]. The Fw.-Kuka, Fw.-Baxter, and Rythmic-Baxter multivariate regression datasets are available from <https://bitbucket.org/athapoly/datasets/src/master/>, and the Sarcos dataset is available from <http://www.gaussianprocess.org/gpml/data/>.

A.7.1 General training details

For all experiments the GP model we fit uses a Matérn 5/2 kernel with individual length scales for each input dimension. For all regression experiments the prior GP mean is a learnable constant; otherwise it is fixed to zero. For all experiments we use the Adam optimizer [Kingma and Ba, 2014]. When training a GP with MLL we set Adam’s momentum hyperparameter β_1 to $\beta_1 = 0.5$; otherwise we set $\beta_1 = 0.90$. We use a stepwise learning rate schedule in which the learning rate starts high (0.03) and is reduced by a factor of 5 every few hundred gradient steps. Our default batch size is $B = 128$, although we use $B = 64$ when the computational demands are higher (e.g. for multi-class classification). We use FAISS for nearest neighbor queries [Johnson et al., 2019]. During training we update nearest neighbor indices every 50 gradient steps, although we note that a smaller update frequency also works well.

To run our experiments we used a small number of GPUs, including a GeForce RTX 2080 GPU, a Quadro RTX 5000, and a GeForce GTX 1080 Ti. We estimate that we used ~ 200 GPU hours running pilot and final experiments.

A.7.2 Details for particular experiments

Model mis-specification The GP prior we use to generate synthetic data has length scale $\rho = \frac{1}{2}$. Note we generate a single data set and then apply different warpings to it; i.e. results for different γ differ only in the warping applied to the inputs.

Objective function comparison Inducing point locations are set using k-means clustering. We retrain SVGP variational parameters for each hyperparameter setting, while keeping the $M = 100$ inducing point locations fixed.

Dependence on number of nearest neighbors k Fig. 3 uses the results reported in Sec. 5.5, with the difference that additional runs with smaller/larger k are included.

Runtime performance To define a regression task we use the Slice UCI dataset and downsample the input dimension to $D = 25$. To accommodate large N we also enlarge the dataset by repeating individual data points and adding noise (both to inputs and targets). We use a mini-batch size of $B = 128$ and run on a GeForce RTX 2080 GPU. As in our other experiments, we update the nearest neighbor index every 50 gradient steps.

Univariate regression Since we reproduce some of the baseline results from [Jankowiak et al., 2020b], we follow the experimental procedure detailed there. In particular regression datasets are centered and normalized so that the trivial zero prediction has a mean squared error of unity. All the experiments in Sec. 5.5-5.8 use training/test/validation splits with proportions 15:3:2. For LOO- k we vary $k \in \{32, 64, 128, 256\}$ and use the validation set LL to choose the best k . SVGP uses $M = 1000$ inducing points with $\beta_{\text{reg}} \in \{0.1, 0.3, 0.5, 1.0\}$ where β_{reg} is a scaling term in front of the KL divergence. PPGPR (specifically the MFD variant, see [Jankowiak et al., 2020b]) uses $M = 1000$ inducing points with $\beta_{\text{reg}} \in \{0.01, 0.05, 0.2, 1.0\}$. Both SVGP and PPGPR results are reproduced from [Jankowiak et al., 2020b]. In both cases inducing point locations are initialized with k -means. For Vecchia and MLL- k we also vary $k \in \{32, 64, 128, 256\}$. For the Vecchia baseline, the data are ordered according to the first PCA vector. For ALC we use the software described in [Gramacy, 2016]. Since prediction is slow, both because the implementation is CPU only and because the iterative procedure is inherently expensive, we use a fixed number of $k = 64$ nearest neighbors. For ALC we use an isotropic kernel on Kegg-undirected because we were unable to obtain reasonable results with a kernel with per-dimension length scales on this particular dataset.

Multivariate regression Since we reproduce some of the baseline results from [Jankowiak et al., 2020a], we follow the experimental procedure detailed there. In particular regression datasets are centered and normalized so that the trivial zero prediction has a mean RMSE of unity (i.e. the RMSE averaged across all output dimensions). For LOO- k we vary $k \in \{16, 32\}$ and use the validation set LL to choose the best k . For MLL- k we vary $k \in \{16, 32\}$. SVGP and PPGPR both use $M = 300$ inducing points with $\beta_{\text{reg}} \in \{0.1, 0.3, 0.5, 1.0\}$.

Binary classification For LOO- k we vary $k \in \{32, 64, 128, 256\}$ and use the validation set LL to choose the best k . For the SVGP and the Pòlya-Gamma PGVI baseline we use $M = 1024$ inducing points and vary $\beta_{\text{reg}} \in \{0.1, 0.3, 0.5, 1.0\}$. We subsample the SUSY and Higgs datasets down to $N = 2 \times 10^5$ data points for simplicity. The Covtype dataset is inherently a multi-class dataset with $K = 7$ datasets. We convert it into two binary classification datasets by combining the two Pine and Fir classes, respectively, in a two-against-five fashion to obtain two derived datasets, Covtype-Pine and Covtype-Fir, respectively. We use $Q = 16$ Gauss-Hermite quadrature points.

Multi-class classification For LOO- k we vary $k \in \{32, 64, 128, 256\}$ and use the validation set LL to choose the best k . For SVGP we use $M = 512$ inducing points and vary $\beta_{\text{reg}} \in \{0.1, 0.3, 0.5, 1.0\}$. We use $Q = 16$ Gauss-Hermite quadrature points.

A.8 Additional figures

In Fig. 8 we replicate the experiment described in Sec. 5.1 for two additional warping functions. In Fig. 9 we depict the results for the multi-class classification experiment in Sec. 5.8.

A.9 Results tables

Tables 6, 7, and 8 report results for all regression and classification experiments from Section 5.

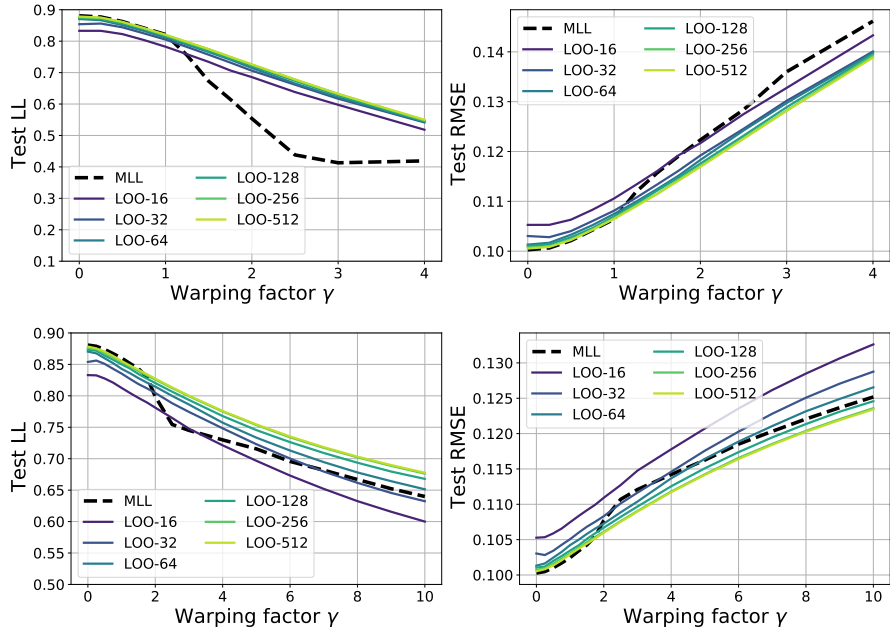


Figure 8: These two figures are companions to Fig. 1 in the main text. We compare predictive performance of a GP trained with a LOO- k objective to a GP trained via MLL, where the GP regressor is mis-specified due to non-stationarity in the dataset introduced by a warping function controlled by γ . **Top:** The coordinatewise warping function is the identity for $x_i \leq 0$ and $x_i \rightarrow x_i^{1+\gamma}$ otherwise. **Bottom:** The coordinatewise warping function is $x_i \rightarrow x_i + \gamma x_i^3$. In both cases as γ increases and the dataset becomes more non-stationary, the LOO- k GP exhibits superior predictive performance, both w.r.t. log likelihood (LL) and root mean squared error (RMSE).

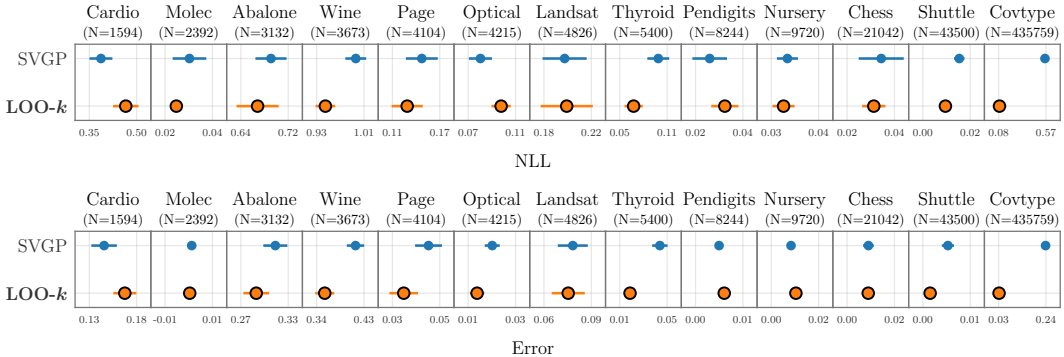


Figure 9: We depict predictive negative log likelihoods (NLL, top) and predictive error (bottom) for 13 multi-class classification datasets using LOO- k and SVGP. Results are averaged over 5 dataset splits. Lower numbers are better.

Table 5: We summarize the performance ranking of LOO- k and SVGP on the multi-class classification datasets in Figure 9, averaged over all splits.

	SVGP	LOO- k
NLL	1.63	1.37
Error	1.68	1.32

Metric	Dataset	SVGP	PPGPR	Vecchia	MLL	ALC	MLL- k	LOO- k
NLL	Pol	-0.651 ± 0.005	-0.825 ± 0.005	-1.190 ± 0.015	-0.817 ± 0.001	-1.696 ± 0.012	-1.200 ± 0.014	-1.238 ± 0.018
	Elevators	0.401 ± 0.007	0.329 ± 0.007	0.407 ± 0.007	0.398 ± 0.013	0.441 ± 0.012	0.397 ± 0.007	0.401 ± 0.008
	Bike	-0.807 ± 0.007	-1.314 ± 0.007	-1.743 ± 0.053	-1.750 ± 0.014	-1.397 ± 0.013	-2.541 ± 0.008	-2.771 ± 0.031
	Kin40K	-0.414 ± 0.002	-0.770 ± 0.002	-0.763 ± 0.002	-0.075 ± 0.001	-0.778 ± 0.003	-0.884 ± 0.002	-1.040 ± 0.030
	Protein	0.902 ± 0.003	0.747 ± 0.008	0.936 ± 0.011	0.875 ± 0.002	0.826 ± 0.020	0.635 ± 0.007	0.626 ± 0.008
	Keggdir.	-1.045 ± 0.017	-1.601 ± 0.016	-1.048 ± 0.016	-0.870 ± 0.052	—	-1.055 ± 0.019	-1.068 ± 0.015
	Slice	-1.267 ± 0.003	-1.516 ± 0.004	-1.648 ± 0.007	-1.240 ± 0.004	-2.441 ± 0.003	-2.572 ± 0.002	-2.753 ± 0.027
	Keggundir.	-0.704 ± 0.006	-1.807 ± 0.018	-0.696 ± 0.004	-0.643 ± 0.008	0.498 ± 0.310	-0.697 ± 0.005	-0.714 ± 0.006
RMSE	Pol	0.107 ± 0.002	0.111 ± 0.002	0.075 ± 0.002	0.074 ± 0.001	0.083 ± 0.001	0.077 ± 0.002	0.073 ± 0.001
	Elevators	0.360 ± 0.003	0.362 ± 0.003	0.362 ± 0.003	0.347 ± 0.007	0.376 ± 0.003	0.359 ± 0.003	0.360 ± 0.003
	Bike	0.088 ± 0.002	0.094 ± 0.002	0.029 ± 0.002	0.022 ± 0.001	0.098 ± 0.002	0.025 ± 0.002	0.028 ± 0.002
	Kin40K	0.147 ± 0.001	0.188 ± 0.002	0.117 ± 0.000	0.084 ± 0.005	0.129 ± 0.001	0.105 ± 0.000	0.095 ± 0.003
	Protein	0.594 ± 0.002	0.609 ± 0.002	0.595 ± 0.007	0.514 ± 0.003	0.571 ± 0.002	0.525 ± 0.002	0.526 ± 0.003
	Keggdir.	0.086 ± 0.001	0.089 ± 0.002	0.085 ± 0.001	0.090 ± 0.004	—	0.085 ± 0.001	0.084 ± 0.001
	Slice	0.051 ± 0.001	0.095 ± 0.001	0.038 ± 0.002	0.031 ± 0.003	0.026 ± 0.002	0.021 ± 0.001	0.024 ± 0.001
	Keggundir.	0.120 ± 0.001	0.124 ± 0.001	0.120 ± 0.001	0.119 ± 0.002	0.118 ± 0.001	0.121 ± 0.001	0.117 ± 0.001
CRPS	Pol	0.061 ± 0.000	0.057 ± 0.000	0.039 ± 0.000	0.051 ± 0.000	0.034 ± 0.000	0.039 ± 0.000	0.036 ± 0.001
	Elevators	0.198 ± 0.001	0.193 ± 0.001	0.199 ± 0.001	0.195 ± 0.003	0.205 ± 0.002	0.197 ± 0.001	0.197 ± 0.001
	Bike	0.049 ± 0.000	0.037 ± 0.000	0.018 ± 0.001	0.019 ± 0.000	0.040 ± 0.000	0.009 ± 0.000	0.008 ± 0.000
	Kin40K	0.082 ± 0.000	0.077 ± 0.000	0.063 ± 0.000	0.093 ± 0.000	0.066 ± 0.000	0.054 ± 0.000	0.047 ± 0.001
	Protein	0.326 ± 0.001	0.310 ± 0.001	0.333 ± 0.004	0.293 ± 0.001	0.285 ± 0.001	0.259 ± 0.001	0.260 ± 0.001
	Keggdir.	0.037 ± 0.000	0.031 ± 0.000	0.038 ± 0.000	0.046 ± 0.002	—	0.037 ± 0.001	0.035 ± 0.000
	Slice	0.031 ± 0.000	0.032 ± 0.000	0.022 ± 0.000	0.029 ± 0.000	0.012 ± 0.000	0.009 ± 0.000	0.009 ± 0.000
	Keggundir.	0.051 ± 0.000	0.036 ± 0.000	0.053 ± 0.000	0.056 ± 0.001	0.033 ± 0.000	0.051 ± 0.000	0.050 ± 0.000

Table 6: A compilation of all univariate regression results from Section 5.5. Numbers are averages \pm standard errors over dataset splits.

Metric	Dataset	SVGP	PPGPR	MLL- k	LOO- k
NLL	Rhythmic-Baxter	-0.003 ± 0.008	-0.087 ± 0.001	-1.123 ± 0.004	-0.911 ± 0.006
	Fw.-Baxter	-1.353 ± 0.001	-1.717 ± 0.001	-1.936 ± 0.001	-1.961
	Fw.-Kuka	-1.060 ± 0.001	-1.557 ± 0.001	-1.892 ± 0.003	-1.886 ± 0.003
	Sarcos	-0.862 ± 0.000	-1.095 ± 0.001	-1.439 ± 0.003	-1.473 ± 0.003
	Rhythmic-Baxter	0.583 ± 0.015	0.609 ± 0.028	0.106 ± 0.001	0.152 ± 0.002
	Fw.-Baxter	0.043 ± 0.000	0.053 ± 0.001	0.035 ± 0.000	0.036
	Fw.-Kuka	0.089 ± 0.000	0.093 ± 0.000	0.115 ± 0.001	0.115 ± 0.001
RMSE	Sarcos	0.105 ± 0.000	0.110 ± 0.000	0.076 ± 0.001	0.077 ± 0.001

Table 7: A compilation of all multivariate regression results from Section 5.6. Numbers are averages \pm standard errors over dataset splits.

Metric	Dataset	SVGP	LOO- k
NLL	Titanic	0.482 ± 0.019	0.483 ± 0.018
	Bank	0.241 ± 0.006	0.246 ± 0.007
	Spambase	0.213 ± 0.004	0.217 ± 0.002
	Musk-2	0.126 ± 0.003	0.114 ± 0.003
	Adult	0.309 ± 0.002	0.319 ± 0.002
	Higgs	0.617 ± 0.002	0.619 ± 0.002
	Susy	0.440 ± 0.001	0.442 ± 0.002
	Covtype-Fir	0.377 ± 0.001	0.354 ± 0.000
	Covtype-Pine	0.381 ± 0.001	0.357 ± 0.001
	Titanic	0.210 ± 0.011	0.209 ± 0.011
	Bank	0.098 ± 0.004	0.102 ± 0.004
	Spambase	0.067 ± 0.002	0.066 ± 0.002
	Musk-2	0.036 ± 0.001	0.033 ± 0.001
Error	Adult	0.142 ± 0.001	0.147 ± 0.002
	Higgs	0.340 ± 0.002	0.341 ± 0.002
	Susy	0.202 ± 0.001	0.205 ± 0.001
	Covtype-Fir	0.171 ± 0.000	0.161 ± 0.001
	Covtype-Pine	0.174 ± 0.001	0.163 ± 0.001
	Cardio	0.387 ± 0.018	0.466 ± 0.020
	Molec	0.030 ± 0.004	0.025 ± 0.001
	Abalone	0.691 ± 0.013	0.668 ± 0.018
	Wine	0.996 ± 0.009	0.945 ± 0.008
	Page	0.147 ± 0.010	0.129 ± 0.010
	Optical	0.080 ± 0.005	0.098 ± 0.004
	Landsat	0.197 ± 0.009	0.199 ± 0.011
	Thyroid	0.099 ± 0.007	0.068 ± 0.006
Error	Pendigits	0.026 ± 0.004	0.032 ± 0.003
	Nursery	0.033 ± 0.001	0.033 ± 0.001
	Chess	0.034 ± 0.005	0.031 ± 0.002
	Shuttle	0.015 ± 0.001	0.010 ± 0.000
	Covtype	0.560 ± 0.002	0.089 ± 0.001
	Cardio	0.146 ± 0.007	0.168 ± 0.006
	Molec	0.001 ± 0.001	0.000 ± 0.000
	Abalone	0.314 ± 0.008	0.289 ± 0.008
	Wine	0.414 ± 0.008	0.355 ± 0.009
	Page	0.045 ± 0.003	0.035 ± 0.003
	Optical	0.020 ± 0.002	0.014 ± 0.002
	Landsat	0.078 ± 0.005	0.075 ± 0.005
	Thyroid	0.044 ± 0.003	0.019 ± 0.002
	Pendigits	0.005 ± 0.000	0.006 ± 0.001
	Nursery	0.008 ± 0.001	0.010 ± 0.001
	Chess	0.009 ± 0.001	0.009 ± 0.001
	Shuttle	0.005 ± 0.001	0.002 ± 0.000
	Covtype	0.238 ± 0.001	0.032 ± 0.000

Table 8: A compilation of all binary (left) and multi-class (right) classification results from Sections 5.7 and 5.8. Numbers are averages \pm standard errors over dataset splits.